Experimental Determination of the Density of States in Nickel*†

ALBERT J. BLODGETT, JR.‡ AND WILLIAM E. SPICER

Stanford Electronics Laboratories, Stanford University, Stanford, California

(Received 6 December 1965)

Energy distributions of photoemitted electrons and the spectral distribution of quantum yield from nickel in the range of photon energy 4.8–11.6 eV are presented and used in conjunction with the optical data of Ehrenreich, Philipp, and Olechna to deduce the electronic structure and optical selection rules of Ni. No evidence is found in these data consistent with the assumption that conservation of $\mathbf{k}$ is an important selection rule. Rather, it is found that first-order agreement is obtained between both the optical and the photoemission data if the optical transition probability is assumed to depend only on the initial and final densities of states. The density of states in the energy regions $-6.0 \leq (E-E_F) \leq 0$ and $5.0 \leq (E-E_F) \leq 11.6$ eV (E_F is the Fermi level) is determined directly from the photoemission data. The density of states in the region $0 \leq (E-E_F) \leq 5.0$ eV is determined using the photoemission results in conjunction with optical data. The most notable feature of the experimentally determined density of states is a strong maximum at 4.6 eV below the Fermi level. Weaker maxima are found at 0.3 and 2.2 eV below E_F. A relatively high density of empty states is found in the conduction band within 0.5 eV of the Fermi level (empty d-like states), and the density of states is approximately constant in the region $0.5 \leq (E-E_F) \leq 11.6$ eV (low-density s- and p-like states). It is shown that the experimentally determined Ni density of states cannot be reproduced from that of Cu via the rigid-band model no matter what value of exchange splitting is chosen.

I. INTRODUCTION

IT has been the purpose of this work to apply the recently developed photoemission techniques to the study of the electronic structure of nickel. Nickel was chosen because it exhibits ferromagnetism, it lies next to copper in the periodic table, and it has the same crystal structure as copper. Berglund and Spicer have previously used photoemission to study the electronic structure of copper.[1]

In recent years, a number of calculations of the energy-band structure of Ni have been made.[2-4] In general, these calculations have been restricted to paramagnetic Ni and have yielded results which suggest that the band structure of Cu[4-6] and of paramagnetic Ni could be related via the rigid-band model (i.e., that the bands of paramagnetic Ni and Cu are similar—only the Fermi levels are different). Several workers have used these calculations and the results obtained from Fermi-surface measurements of Cu and Ni to estimate the position and nature of the bands in ferromagnetic Ni.[7,8] However, the paucity of definitive experimental data away from the Fermi surface has made it very difficult to check the validity of the approximations used in the

various theoretical models. By making use of the density of states determined from photoemission studies of Cu[1] and the results of this investigation, the rigid-band model could be tested over the complete extent of the conduction band.

II. THEORY AND METHODS FOR ANALYSIS OF DATA

Photoemission may be considered a three-step process: first, electrons are photoexcited to higher energy states; second, a portion of the photoexcited electrons diffuse to the surface; and third, a portion of the photoexcited electrons arriving at the surface escape over the surface barrier into the vacuum. In travelling to the surface, the excited electrons may suffer elastic or inelastic collisions. Experimentally, it is possible to measure the spectral distribution of quantum yield in electrons per incident photon (abbreviated here to the SDQY) and the energy distribution of the photoemitted electrons (frequently referred to as the energy distribution curve: EDC). The principal object of this work is to determine the optical transition probability $P(\hbar\omega, E)$ as a function of the energy of the initial (or final) state and the energy of the exciting photons. From $P(\hbar\omega, E)$ obtained over a wide energy range, information on the structure of electronic states and the optical selection rules may be derived. If there were no inelastic scattering of the electrons before escape and if the probability of escape for each electron reaching the surface were independent of energy, the optical transition probability $P(\hbar\omega, E)$ would be directly proportional to the number of electrons emitted with energy, E, for photon energy, $\hbar\omega$, i.e., it could be obtained directly from the EDC's. In general, it is possible in the analysis of the data to separate to a large degree the effects due to optical transitions (i.e., the first step) and those due to scattering and escape. In this discussion, we will first treat the procedure by which information concerning the electronic states may be

* Work supported by the National Science Foundation, and by the Advanced Research Projects Agency through the Center for Materials Research at Stanford University.

† Based on thesis submitted by A. J. Blodgett, Jr., to Stanford University in partial fulfillment of the requirements of the Ph.D. degree.

‡ IBM Resident Fellow. Present address: IBM Components Development, Hopewell Junction, New York.

[1] C. N. Berglund and W. E. Spicer, Phys. Rev. **136**, A1044 (1964).

[2] J. G. Hanus, MIT Solid State Molecular Theory Group Quarterly Progress Report No. 44, 1962 (unpublished).

[3] J. Yamashita, M. Fukuchi, and S. Wakoh, J. Phys. Soc. Japan **18**, 999 (1963).

[4] L. F. Matthesis, Phys. Rev. **134**, A970 (1964).

[5] B. Segall, Phys. Rev. **125**, 109 (1962).

[6] G. A. Burdick, Phys. Rev. **129**, 138 (1963).

[7] H. Ehrenreich, H. R. Philipp, and D. J. Olechna, Phys. Rev. **131**, 2469 (1963).

[8] J. C. Phillips, Phys. Rev. **133**, A1020 (1964).

obtained from the photoemission data in the absence of inelastic scattering. This treatment will be followed by a discussion of the problems which arise due to inelastic scattering and the procedures used to minimize the effect of scattering in deriving the density of states.

In order to obtain information on the electronic states from optical data, the optical selection rules must be known. It is customarily assumed that the most important optical selection rule in crystalline solids is that requiring direct conservation of crystal momentum, $\hbar\mathbf{k}$. In recent papers based upon photoemission studies of various materials,[1,9,10] Spicer, Berglund, and Kindig have indicated that it is possible to determine whether or not conservation of wave vector $\mathbf{k}$ is an important selection rule for optical transitions in a solid by studying the behavior of structure in EDC's taken over a large range of photon energy. In these papers[1,9,10] the optical transitions have been considered in two groups—direct transitions in which wave vector $\mathbf{k}$ is conserved directly and nondirect transitions which consist of all other transitions.

Berglund and Spicer (see p. A1040 of Ref. 10) have pointed out that it is very difficult to determine experimentally whether or not direct conservation of $\mathbf{k}$ is an important selection rule in cases where bandwidths are comparable with the resolution (0.1–0.2 eV) obtainable in the energy distribution measurements. Clearly, in the limit of negligible bandwidth, all values of $\mathbf{k}$ are degenerate in energy, and $\mathbf{k}$ conservation loses importance as an optical selection rule. In order to avoid confusion over this point, a pragmatic approach will be used in this paper. If no evidence can be found in the photoemission data that direct conservation of $\mathbf{k}$ is an important selection rule, the transition will be said to belong to the class of KNIMP ($\mathbf{k}$ not important) transitions. This should remove the ambiguity which might arise for narrow bands.

Since it was found that the Ni data could be explained in terms of KNIMP transitions with constant-momentum matrix elements,[10] the model which assumes these properties is discussed here in detail. In Sec. V, it will be shown that this interpretation is consistent with the experimental data.

If KNIMP transitions are dominant and the matrix elements are constant to the first approximation, the transition probability will be determined by the densities of states at the energies of the initial and final states.[10] To illustrate the first step (photoexcitation) in the photoemission process under these conditions, consider a hypothetical metal with the density of states shown in Fig. 1. If this material is illuminated with photons of energy $\hbar\omega$, each state in the valence band is coupled to a state in the conduction band $\hbar\omega$ above it in energy. It is convenient to shift the valence-band density of states N_V by $\hbar\omega$ in energy to line up corre-

[9] N. B. Kindig and W. E. Spicer, Phys. Rev. 138, A561 (1965).
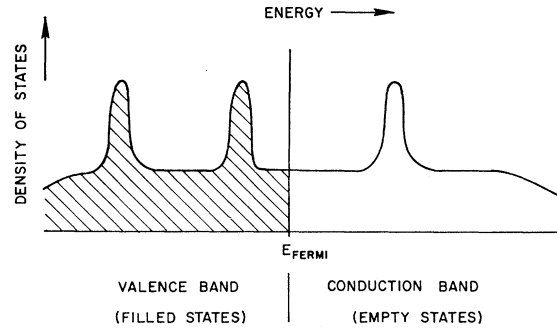[10] C. N. Berglund and W. E. Spicer, Phys. Rev. 136, A1030 (1964).

FIG. 1. The density of states of a hypothetical metal.

sponding pairs of coupled states as shown in curves (a) and (b) of Fig. 2. If the momentum matrix elements coupling each pair of optically coupled states are assumed equal and conservation of $\mathbf{k}$ is unimportant, the distribution in energy of photoexcited electrons inside the material is simply the product of curves (a) and (b) as indicated by curve (c) of Fig. 2.

After excitation, the electron must move through the crystal before it can arrive at the surface and escape into vacuum. This motion is the second step in the photoemission process. Here, the excited electron can be scattered. The possible effects of such scattering will be discussed in Sec. V.

In the third step of the photoemission process, those photoexcited electrons which reach the surface of the metal with sufficient momentum in the direction perpendicular to the surface escape into the vacuum. The restriction imposed on escape by the potential barrier at the surface may be taken into account by the escape function $T(E)$ as indicated in curve (d) of Fig. 2. Because of the complexity of the band structure of the material and of the surface effects (not fully understood) that affect $T(E)$, no attempt will be made to calculate
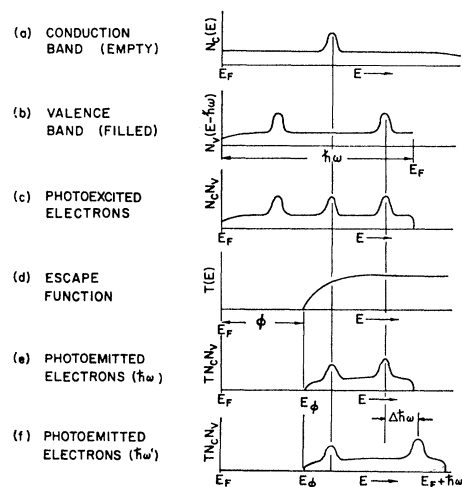

FIG. 2. Diagram illustrating the relationship between the density of states and the energy distributions of photoemitted electrons when conservation of wave vector $\mathbf{k}$ is not an important selection rule and when momentum matrix elements are constant.

$T(E)$ directly; $T(E)$, however, will be determined from the experimental data (see Sec. VA).

In the present approximation, it is evident that the energy distribution of photoemitted electrons $\mathfrak{N}(E)$ is given by Eq. (1) as indicated by curve (e) of Fig. 2.

$$\mathfrak{N}(E)=CT(E)N_C(E)N_V(E-\hbar\omega). \tag{1}$$

Here C is a constant. The energy of the vacuum level is denoted by E_φ in Fig. 2 and is related to the work function φ and the Fermi energy E_F by

$$\varphi=E_\varphi-E_F. \tag{2}$$

The zero-kinetic-energy point on an EDC is that point at which the retarding potential used in the measurement[11] is equal to zero. The position of this point on an EDC depends upon the difference between the emitter work function and the collector work function. In this work, the phototubes were designed with Ni deposited on both collector and emitter so that collector and emitter work functions are identical. When this is the case, the zero-kinetic-energy point occurs at the vacuum energy E_φ as indicated in curve (e) of Fig. 2.

There are two peaks in curve (e) of Fig. 2—one corresponding to a high-density point in the valence band and one corresponding to a high-density point in the conduction band. Which part of the observed structure is due to N_V and which part is due to N_C cannot be determined from a single EDC; however, this can be determined from two EDC's. If the hypothetical material considered here is studied with photons of a particular energy $\hbar\omega$ and then with photons of higher energy $\hbar\omega'$, the peak in the EDC due to a high-density peak in N_V would move in energy by an amount exactly equal to the increase in photon energy—$\Delta\hbar\omega=\hbar(\omega'-\omega)$ —as indicated by curve (f) of Eq. (3), since the initial state (as opposed to the final state) for these transitions is independent of $\hbar\omega$.

$$E_{\text{structure}}=\hbar\omega-E_{\text{sv}}. \tag{3}$$

Here E_{sv} is the energy of the corresponding structure in N_V. In contrast, the peak in the EDC due to structure in N_C would maintain a constant position in energy, as shown by curve (f) and indicated by Eq. (4), since the final state is independent of $\hbar\omega$.

$$E_{\text{structure}}=E_{\text{sc}}. \tag{4}$$

Here E_{sc} is the energy of the structure in the conduction band. If structure in an EDC moves in energy by an increment less than the change in photon energy—i.e., if it does not obey Eqs. (3) or (4)—it is due to direct transitions and the model described here is invalid.[10]

The discussion above is based on the assumption of no inelastic scattering. [Except for possible effects on $T(E)$ and indirect effects on optical-transition probabilities, elastic scattering does not affect the shape of the EDCs since there is no energy loss involved.] It remains

to examine the possible effects of inelastic scattering on the energy distributions. For our purposes here, phonon scattering can be considered elastic since the energy loss per collision (0.03 eV) is small compared to the resolution of approximately 0.1 eV of these experiments. Only electron-electron scattering need be treated as inelastic. Berglund and Spicer[1,10] have treated such scattering in Cu in detail using simple assumptions. Their results indicate the following: (1) The scattering probability, and thus the number of scattered electrons, increases with increasing electron energy. (2) Even when strong structure is present in the valence band of a metal, the contribution to EDC's due to inelastically scattered electrons is essentially without structure and peaks near zero kinetic energy. (3) The energy of the peak due to scattered electrons does not change with increasing $\hbar\omega$; however, the number of electrons in the scattered distribution does increase with increasing $\hbar\omega$. (4) Structure in energy distributions, due to valence-band structure, which is sharp at lower values of photon energy will be broadened by scattering at higher photon energies. The first point has also been well established in other work.[12] There is strong experimental evidence to support the second and third points both in metals[1] and in semiconductors.[9] In analyzing the experimental data, use will be made of these characteristics of inelastically scattered electrons in separating the effects of scattering from the effects of density of states. Provided it is constant in energy, the scattering peak does not obey Eq. (3), and therefore, cannot be mistakenly attributed to structure in the valence band. Although the scattering peak will obey the energy relation given by Eq. (4), it can be distinguished from structure in the conduction-band density of states since it will appear only when scattering becomes important and will then increase monotonically with increasing $\hbar\omega$ without any appreciable shift of the energy at which the maximum appears. In general, when scattering does occur, its effect is smallest at low photon energies, and therefore, the EDC's taken at low photon energies can be used to determine the conduction-band density of states in the low-energy region—the region which may be obscured by scattering in EDC's taken at higher photon energies.

The structure in the EDCs presented in a later section (Sec. IVB) is shown to be due principally to valence-band structure. This can be established most easily by plotting the energy distributions not against E (the kinetic energy of the emitted distributions), but against $(E-\hbar\omega)$ where $\hbar\omega$ is the energy of the emitted photons. In this way, the energy distributions are referred to the energy of the initial state[13] with the zero of energy taken at the vacuum level. When the structure in the EDC's is due to valence band, it will coincide on a $(E-\hbar\omega)$ plot independent of $\hbar\omega$.

[11] W. E. Spicer and C. N. Berglund, Rev. Sci. Instr. 35, 1665 (1964) and references given therein.

[12] L. Apker, E. A. Taft, and J. Dickey, J. Opt. Soc. Am. 43, 78 (1953); W. E. Spicer, J. Phys. Chem. Solids 22, 365 (1961); N. B. Kindig and W. E. Spicer, Phys. Rev. 138, A561 (1965).

[13] W. E. Spicer, Phys. Rev. Letters 11, 243 (1963).

III. EXPERIMENTAL METHODS

Many of the experimental methods and techniques used in this work have been reported in the literature,[11,14] and for this reason, they are only outlined here. In general, the experimental data were obtained from sealed-off vacuum phototubes that were provided with LiF windows having a high-energy cutoff at 11.6 eV. The nickel samples were formed by evaporation from Ni-plated tungsten helices. The SDQY's for the Ni samples were obtained using standard techniques,[15] and the EDC's were obtained using the ac method described by Spicer and Berglund.[11] Measurements in the vacuum ultraviolet were made using a McPherson monochromator with a hydrogen arc as the source.

Attempts were made to lower the work function of Ni, and thereby extend the range of measurements, by depositing approximately a monolayer of Cs on the Ni surface. This method has been used successfully on Cu and Ag.[1] However, these attempts failed due to the formation of a Ni-Cs alloy. The variation observed in the photocurrent of the sample during the cesiating process indicated that Cs was diffusing into the Ni sample[16]; further, the data obtained from cesiated Ni samples were not consistent with those obtained from atomically clean Ni.[16] For this reason, only the data obtained from atomically clean Ni are presented in this paper.

Some Ni samples were prepared in a continuously pumped high-vacuum chamber to allow study of Ni above its Curie temperature. The VacIon system used in this work has been described by Kindig and Spicer.[14] For these studies the substrates upon which the Ni films were evaporated were fitted with small heaters formed from tantalum wire. In general, these high-temperature studies have proved difficult due to anomalous thermionic emission and problems encountered in preparing Ni samples suitable for high-temperature studies.[16] The problems encountered were Ni peeling off the substrate at elevated temperatures and alloying of the Ni with the Cu substrate. Because of these difficulties, only preliminary and incomplete high-temperature data are presently available; however, high-temperature studies will be continued in this laboratory.

IV. PRESENTATION OF DATA

A. The Quantum Yield

The spectral distribution of the quantum yield (SDQY) of nickel is shown in Fig. 3. This curve has been corrected for the transmission of the LiF window used for the phototube and for the reflectivity of nickel.[7] The work function φ of nickel is obtained from
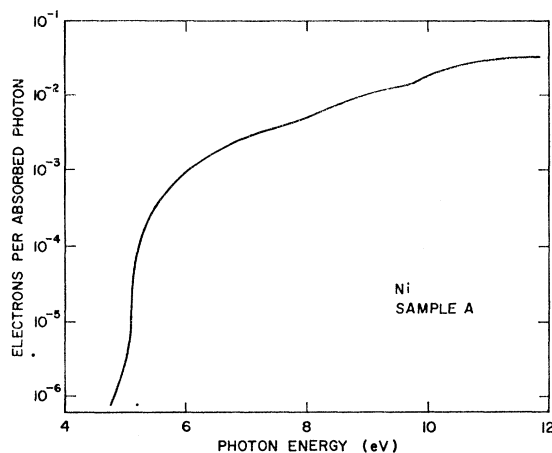

FIG. 3. The spectral distribution of the quantum yield of nickel.

the SDQY by using a method described by Fowler.[17] Using this method, the quantum yield Y of metals may be approximated near threshold by[1]

$$Y(\hbar\omega) = A(\hbar\omega - \varphi)^2, \quad \hbar\omega > \varphi \qquad (5)$$
$$0, \quad\quad\quad\quad \hbar\omega \leq \varphi.$$

Here A is a constant. Therefore, the square root of the quantum yield (near threshold) plotted against photon energy should be a straight line which intersects the energy axis at $\hbar\omega = \varphi$. The square root of $Y(\hbar\omega)$ for nickel, shown in Fig. 4, may be approximated by two straight lines corresponding to two different work functions with values 4.5 and 5.0 eV. (This result is in reasonable agreement with the bivalued work function for nickel of 4.4 and 4.8 eV reported by Wilson.[18]) The relative size of the low-energy segment was observed to vary somewhat from sample to sample, but the intercept was approximately the same for all samples. The work of Surhman and Wedler[19] suggests that the low-energy
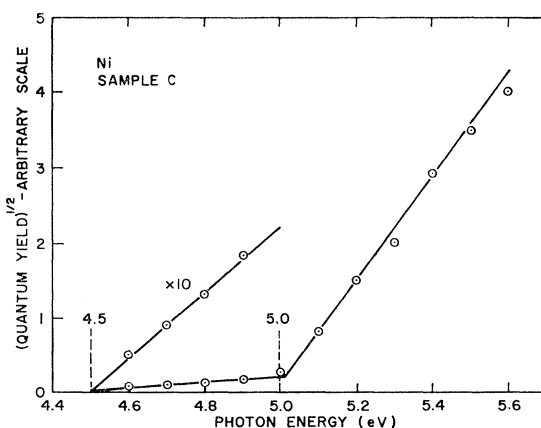

FIG. 4. Evaluation of the work function of nickel.

[14] N. B. Kindig and W. E. Spicer, Rev. Sci. Instr. 36, 759 (1965).
[15] N. B. Kindig, Ph.D. dissertation, Stanford University, 1964 (unpublished).
[16] A. J. Blodgett, Jr., Ph.D. dissertation, Stanford University, 1965 (unpublished).

[17] R. H. Fowler, Phys. Rev. 38, 45 (1931).
[18] R. G. Wilson, Bull. Am. Phys. Soc. 10, 432 (1965).
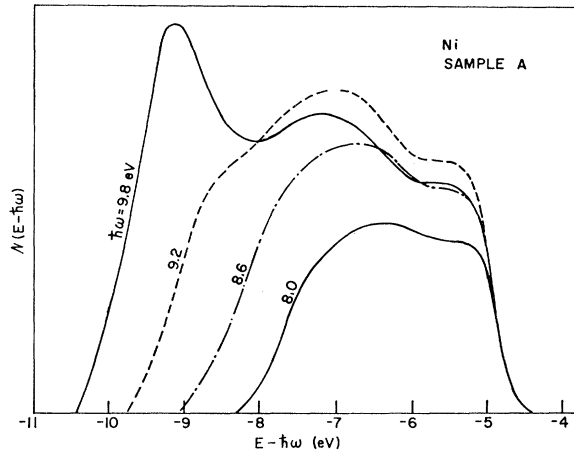[19] V. R. Suhrman and G. Wedler, Z. Angew. Phys. 14, 70 (1962).

FIG. 5. Energy distributions of photoemitted electrons from nickel plotted versus $E-\hbar\omega$, for $\hbar\omega \leq 9.8$ eV.

segment may be due to an unordered phase of Ni and the high-energy segment because of the ordered phase.[20] Since the value (5.0 eV) of work function corresponding to the high-energy segment accounts for over 99% of the photoemitted electrons for photon energies at which EDC's were obtained, this value is used in the analysis of the data.

B. The Energy-Distribution Curves

The EDC's are related to the SDQY in that the area under each EDC (i.e., the total number of photoemitted electrons) is proportional to the quantum yield at the corresponding photon energy. It is therefore possible to assign relative amplitudes to a set of EDC's by making the area under each EDC proportional to the SDQY at the corresponding photon energy, using the same constant of proportionality for all curves. Energy distribution curves which have been normalized to the yield
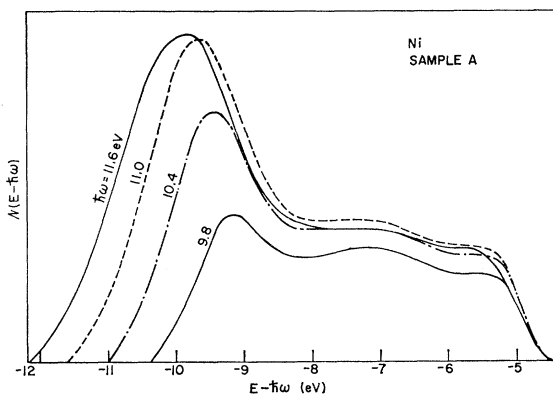

FIG. 6. Energy distributions of photoemitted electrons from nickel, plotted versus $E-\hbar\omega$, for $\hbar\omega \geq 9.8$ eV.

[20] Suhrman and Wedler (Ref. 19) discuss these phases of nickel and list 12 values of work function for unordered Ni ranging from 4.54 to 4.61 eV and 12 values for ordered Ni ranging from 4.76 to 5.28 eV.
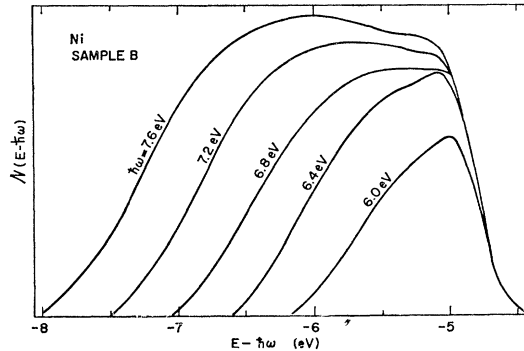

FIG. 7. Energy distributions of photoemitted electrons from nickel, plotted versus $E-\hbar\omega$, for $\hbar\omega \leq 7.6$ eV.

will be called NEDC's here (normalized EDC's). This normalization process is useful in the analysis of the EDC's. Consider, for example, a material in which the conduction-band density of states is constant and for which the model discussed in Sec. II (i.e., KNIMP transitions and constant momentum matrix elements) is valid. NEDC's for such a material will superimpose when plotted versus $E-\hbar\omega$, and the observed structure is a replica of the valence-band density of states. This interpretation is discussed below in more detail in conjunction with the experimental data.

A typical set of NEDC's is shown in Figs. 5 and 6. The low-energy portion of each curve in these figures is reduced by the escape function $T(E)$ (see Fig. 2). A small peak which suggests a weak maximum in the valence-band density of states occurs in each NEDC (Figs. 5 and 6) at approximately -5.3 eV. A broader peak at approximately -7.2 eV is slowly uncovered as $\hbar\omega$ is increased to 9.8 eV.[21] Both of these peaks may be broadened by lifetime broadening.

The NEDC's (Figs. 5–7) provide the most important portion of the information obtained from photoemission studies on Ni. Several important features of the electronic structure and optical selection rules for Ni are suggested by the essential superimposition of NEDC's for the range 6.0 eV $< \hbar\omega \leq 11.6$ eV[22] in which data may be obtained for atomically clean Ni under good vacuum.

[21] The relative amplitudes of the NEDC's in Fig. 5 is a source of minor concern. Since these curves are normalized to the yield, one would expect the NEDC's to superimpose between -6 and -5 eV. The observed deviation from ideal behavior is in the wrong direction to be due to electron-electron scattering—such inelastic scattering would cause the number of high-energy electrons to decrease as the photon energy is increased (see Sec. II). (On the other hand, the slight shift observed in the shoulder near -5.3 eV is probably due to such scattering processes.) It is most probable that this discrepancy is due to an error in the SDQY. An error of approximately 30% between photon energies of 8.0 and 9.8 eV, which is not too significant on a semilog plot, can explain this deviation. This error could be due to an error in the measurement of the source intensity spectrum (likely), an error in determining the transmission of the LiF window (unlikely), or an error in the reflectivity data (unlikely since the total reflectance is only $\approx 20\%$ in this range of photon energy).

[22] Again the relative amplitude of the 9.8 eV curve is probably erroneous. The major point here is that the NEDC's have the same shapes in this energy range.

[The escape function, see Fig. 10, affects the energy distribution for final energies within one or two electron volts of the vacuum level, see Eq. (1). The effect of this is apparent near the minimum energy of each curve in Figs. 5–7.] (The escape function, see Fig. 10, rises within a few electron volts of the threshold energy for emission. The result of this is apparent in Figs. 5–7.)

First, KNIMP transitions dominate the optical property in Ni for $6.0 \leq \hbar\omega \leq 11.6$ eV. This is deduced from the fact that the data obey Eq. (3).

Second, since all of the observed structure obeys Eq. (3), the density of states (in the corresponding energy range) in the conduction band must be approximately constant, and the shape of the EDCs in this region must be determined to the first approximation by the valence-band density of states.

Third, the assumption that the momentum matrix elements coupling each pair of optically coupled states are equal is consistent (at least in the first-order approximation) with these results. A deviation from constant matrix elements would prevent superimposition of the curves in Figs. 5–7 [see Eq. (1)]; therefore, an upper limit of the variation in matrix elements may be obtained by noting the lack of absolute superimposition.[23] However, much of the lack of deviation from superimposition may be explained by the escape function, effects of scattering, and difficulty in determining the absolute quantum yield. These effects are discussed elsewhere in this article.

The structure in the NEDC's (Fig. 6) below −8 eV is due to a high-density peak in N_V which is slowly uncovered as $\hbar\omega$ is increased. Because of the $T(E)$ effect in all of the curves and because of some scattering effects in the EDC's taken at $\hbar\omega \geq 11.0$ eV, it is particularly difficult to determine the exact shape of this peak by inspection; however, it will be determined (see Sec. VA) by using the method of analysis described in Sec. II.
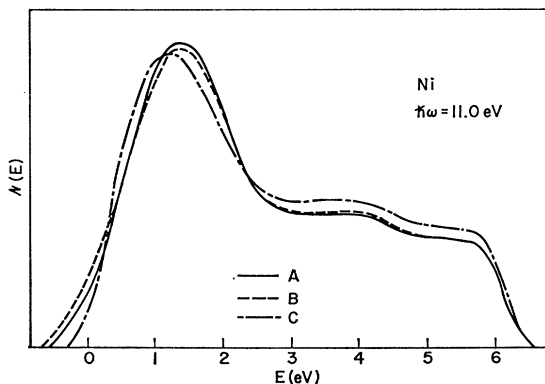

FIG. 9. Energy distributions of photoemitted electrons from samples A and B at $\hbar\omega = 8.6$ eV.

The features of the electronic structure and optical selection rules suggested above for $6.0 \leq \hbar\omega \leq 11.6$ eV can be checked for $1.0 \stackrel{\sim}{\leq} \hbar\omega \leq 7$ eV by calculation of the optical constant $\sigma\omega$ once the conduction-band states below the vacuum level have been determined. This is done in Sec. VC and reasonable agreement is found between the calculated and measured $\omega\sigma$ curves.

C. Reproducibility of Data

Three sets of data were obtained from Ni samples (without Cs) at room temperature. Sets A and B were obtained from the same tube and set C was obtained from a different tube. The NEDC's in Figs. 5 and 6 are taken from set A which was obtained just after the tube preparation. The NEDC's in Fig. 7 are taken from set B which was obtained six months after set A, when modification of equipment allowed measurement of EDC's at photon energies as low as 6 eV.

The energy distributions obtained at $\hbar\omega = 11$ eV from each set of data are shown in Fig. 8. These curves have been arbitrarily set equal near 2 eV for sake of comparison.[24] In general, the reproducibility of the data from sample to sample is very good. The variation

FIG. 8. Energy distributions of photoemitted electrons from various nickel samples at $\hbar\omega = 11.0$ eV.

FIG. 10. Curves illustrating the variation observed in the escape function.

---

[23] It is possible, but very unlikely, that both the momentum matrix elements and the conduction-band density of states vary with $\hbar\omega$ but in such a manner that the variations cancel out.
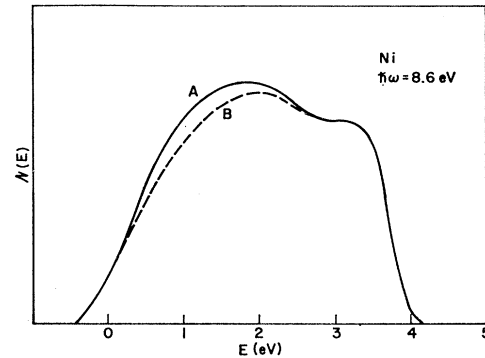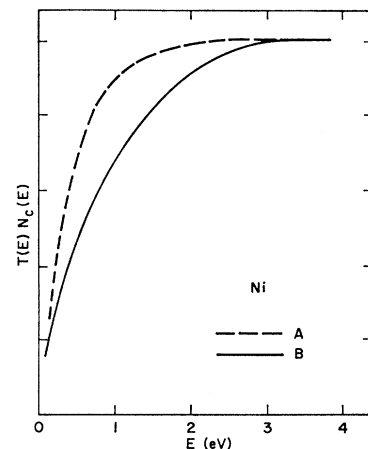
[24] These curves were not normalized to their respective yields because of inadequate data.
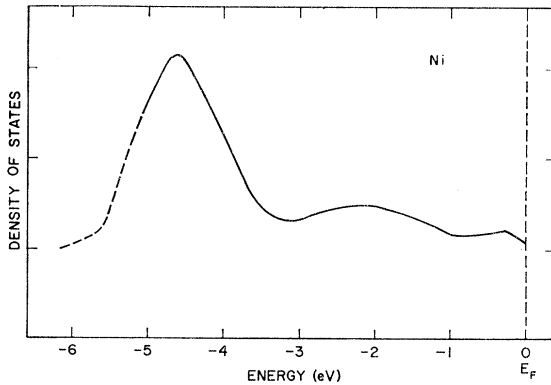
FIG. 11. The valence-band density of states in nickel as determined by photoemission studies.

observed in these curves (Fig. 8) near 1 eV is attributed in part to variations in the escape function (see below) and in the number of scattered electrons. The variation in the low-energy zero intercept may be related to the nonuniformity in work function which affects the SDQY near threshold (see Sec. IVA).

In order to illustrate more clearly the difference between sets A and B, a second pair of EDC's from these sets is shown in Fig. 9. The observed differences between the EDC's in sets A and B (Figs. 8 and 9) is attributed to a slow variation (approximately 20% in 6 months) in the escape function. The variation in $T(E)$ can be shown by calculating the product $T(E)N_C(E)$ from the different sets of EDC's by methods discussed in Sec. II; this calculation is discussed in more detail in Sec. VA. The $T(E)N_C(E)$ so determined from sets A and B are shown in Fig. 10. It seems reasonable to assume that the observed variation is due to a change in $T(E)$ caused by aging of the surface.

The low- and high-energy cutoffs of the present energy distributions are not absolutely sharp. For example, some electrons appear in Fig. 8 at negative energies and some above 6.0 eV (since $\hbar\omega = 11.0$ eV and $\varphi = 5.0$ eV, the maximum energy of photoemitted electrons should be 6.0 eV). As this is due to the finite resolution characteristic to the determination of EDC's, it is common, in varying degrees, to all experimentally determined EDC's. Most important among the factors which prevent the upper and lower energy cutoffs from being absolutely sharp are: (1) the finite bandwidth of the monochromator (in the present experiment $\Delta\hbar\omega = 0.2$ eV at 11 eV and was smaller at lower $\hbar\omega$); (2) the finite bandwidth of the system which measures the energy distributions (in the present experiment this bandwidth was set by the magnitude, 0.1 V or less peak to peak, of the modulating ac signal); and (3) any variations in the emitter and/or collector work functions.

D. High-Temperature Data

Several EDC's were taken at $\hbar\omega = 10.2$ eV at room temperature and at approximately 400°C (the Curie

temperature of Ni is 358°C). The low-energy peak (i.e., the peak near 1 eV—see Fig. 8) is obscured in these data by thermionic and other effects. However, the two peaks which occur at higher energies are well resolved. This structure occurs at the same energy within ±0.2 eV in both the room temperature and the 400°C curves, indicating that the densities of states of ferromagnetic and paramagnetic Ni are quite similar.

Because of the difficulties inherent in these measurements,[16] the present data are only preliminary—these studies will be continued in this laboratory.

V. DETERMINATION OF THE DENSITY OF STATES

A. The Density of States below the Fermi Level and above the Vacuum Level

It was shown in the previous section that the major structure observed in the NEDC's is due to structure in N_V. It was also pointed out that the major peak observed near -10 eV in Fig. 6 contains a contribution due to scattering. Since (see Sec. II) a scattering peak typically maintains a constant position in energy and since structure due to N_V moves in energy as photon energy is increased, the analysis based upon Eq. (1) separates these two contributions.

The valence-band density of states determined by the analysis based on Eq. (1) is shown in Fig. 11. The major portion of this curve was determined from the 10.2- and 10.4-eV EDC's of set A. The EDC's taken at lower
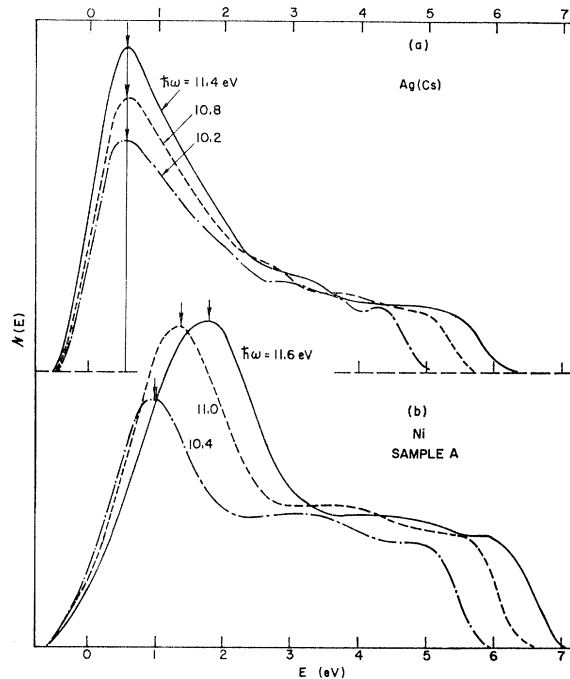

FIG. 12. Energy distributions of photoemitted electrons; (a) silver with cesium on the surface, after Berglund and Spicer (Ref. 1); (b) nickel.
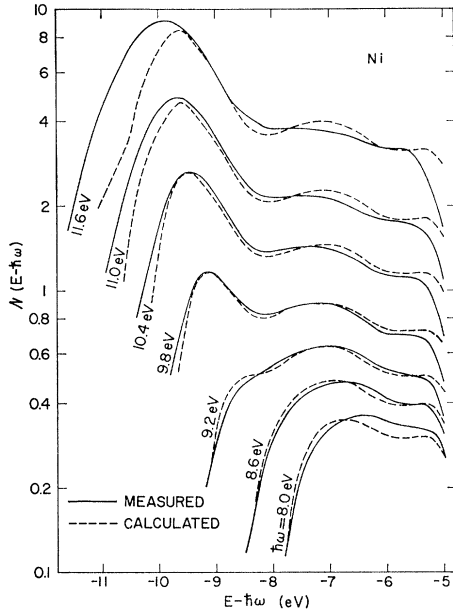
FIG. 13. Calculated and measured energy distributions of photo-emitted electrons from nickel.

photon energies were used to determine the exact shape in the region between -1 and 0 eV, because the effects of scattering are reduced at the lower energies, and EDC's taken at higher photon energies were used to determine N_V in the region $(E-E_F)\le -5$ eV, i.e., for energies below the maximum in density of states at about 4.6 eV. Based upon the agreement between measured and calculated EDC's (see following section) in this region, the density of states (Fig. 11) is estimated to be accurate within $\pm 10\%$ in the region of $-5 \le (E-E_F)\le -0.5$ eV. However, broadening effects due to scattering,[1,10] may produce an effective decrease in the magnitude of maxima in the density of states.

Since the large peak in the Ni density of states, which occurs at about 4.6 eV below the Fermi surface (see Fig. 11), will play an essential role in the interpretation of the electronic structure of Ni, it is important to be sure that this peak is a result of the Ni density of states and that it is not an artifact produced by the presence of inelastically scattered electrons in the energy distributions. In the following sections, this will be checked by using the valence-band density of states to calculate (1) energy distributions for a wide range of photon energies (Sec. VB), and (2) the optical constant $\omega\sigma(\omega)$ (Sec. VC). To contrast the behavior of a scattering peak and that of the peak observed for Ni, NEDC's for Ag (obtained from Berglund and Spicer's data[1]) and for Ni are shown in Fig. 12. These curves have not been shifted by $\hbar\omega$ and, hence, are referred to the final states of the photoemitted electrons. The low-energy peak in the Ag data is due to scattered electrons.[1] It is clear that this peak maintains a constant position in energy and that its amplitude increases with photon energy. In

contrast, the low-energy peak in the Ni data [Fig. 12(b)] clearly moves in energy as $\hbar\omega$ is varied. This peak does not move directly as $\hbar\omega$ because of the effects of escape function (particularly in the 10.4-eV EDC) and scattering (particularly in the 11.6-eV EDC). The escape function (see Fig. 10) can cause an effective shift towards higher energy. The contribution to the low-energy peak in the Ni data due to scattering is indicated quantitatively in Sec. VB when the measured and calculated EDC's are compared.

The method based upon Eq. (1) which was used to determine the valence-band density of states (Fig. 11) was also used to determine the product $T(E)N_C(E)$ from the 9.0- and 9.2-eV EDC's of data sets A and B. The results (Fig. 10) were discussed earlier in Sec. IVC. This detailed analysis suggests that the conduction-band density of states is approximately constant above the vacuum level. The decrease in magnitude of $T(E)N_C(E)$ at lower energies is that which would be expected from $T(E)$ alone; however, there is no direct method by which a separation of the terms $T(E)$ and $N_C(E)$ may be made in this work.

B. The Calculated Energy Distribution Curves

Since the density of states (Fig. 11) and the escape function (Fig. 10) were determined using only limited data [$N(E)$ was derived principally from the 10.2- and 10.4-eV EDC's, $T(E)$ was derived from the 9.0- and 9.2-eV EDC's], it is possible to check the assumptions (KNIMP transitions and constant-momentum matrix elements) upon which the analysis is based by using $N(E)$, $T(E)$, and Eq. (1) to calculate a number of EDC's between 8.0 and 11.6 eV. The EDC's so calculated are compared with the measured EDC's in Fig. 13. The relative amplitudes of the measured and calculated curves at each $\hbar\omega$ have been arbitrarily set equal at one value of $(E-\hbar\omega)$. The two sets of curves are in reasonable agreement. The differences which do exist between the two sets are probably caused by the effects of inelastic scattering (see Sec. II) and of momentum matrix elements that are not completely constant. Scattering will reduce the number of high-energy electrons and increase the number of low-energy electrons. These effects will increase in magnitude with increasing photon energy.[10] Evidence for a systematic loss of high-energy electrons can be seen in Fig. 13. This effect is most pronounced in the high-energy peak near -5.3 eV and is noticeable in the peak near -7.2 eV. An enhanced number of low-energy electrons is particularly noticeable for $\hbar\omega\le 11.0$ eV at the low-energy sides of the peaks at -9.6 and -7.2 eV.

C. The Density of States between the Fermi Level and the Vacuum Level

In order to determine the approximate density of states between the Fermi level E_F and the vacuum level E_φ, it is useful to consider first the electronic structure of
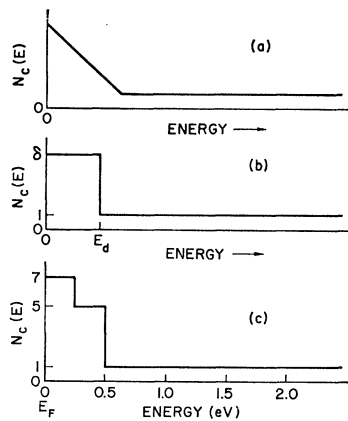
Fig. 14. Various esti-
mates of the conduction-
band density of states,
near the Fermi level, in
nickel.

Fig. 15. The optical conductivity multiplied by ω; solid curve is after Ehrenreich, Philipp, and Olechna (Ref. 7); dashed curve is calculated on basis of KNIMP transitions, constant matrix elements, and Ni density of states (Fig. 18).

Ni. Atomic Ni has ten outer (i.e., noncore) electrons— nine $3d$ electrons and one $4s$ electron; however, Ni in solid ferromagnetic form is generally attributed to have approximately 9.4 $3d$-like and 0.6 $4s$-like electrons.[25] Therefore, 0.6 $3d$-like holes will be present in the conduction band. In general, d-like states are characterized by high density in energy and s- and p-like states are characterized by low density.[1] Therefore, it is probable that the major portion of the density of states shown in Fig. 11 is due to $3d$-like states, and further, it is reasonable to assume that these states are approximately continuous through the Fermi energy. Once the unfilled d-like states have been taken into account, the density of states in the conduction band drops to a lower level corresponding to the lower density s- and p-like states. The constant $N(E)$ observed above the vacuum level is undoubtedly due to these types of states. These considerations suggest that $N_C(E)$ might be approximated by one of the forms shown in curve (a) or (b) of Fig. 14.

A more exact form of $N_C(E)$ in this region can be determined using the optical conductivity. The optical conductivity $\sigma(\omega)$ in terms of the model used in this work is given by

$$\sigma(\omega) = \frac{B}{\omega} \int_{E_F}^{E_F - \hbar\omega} N_C(E) N_V(E - \hbar\omega) dE. \qquad (6)$$

Here B is a constant. Since N_V has been derived in this work, and $\sigma(\omega)$ has been derived from reflectivity data by Ehrenreich, Philipp, and Olechna,[7] it is possible to determine N_C between E_F and E_φ using Eq. (6). Various $N_C(E)$ were used to calculate $\omega\sigma(\omega)$ by this method, and the closest agreement between $\omega\sigma(\omega)$ so calculated from the density of states and that derived (by Kramers-Kronig analysis) from the reflectance[7] was obtained using the $N_C(E)$ shown by curve (c) of Fig. 14. This calculation is discussed in detail in the Appendix. The two $\omega\sigma(\omega)$ curves are shown in Fig. 15; these curves have been normalized at 4.9 eV. The $\omega\sigma(\omega)$ curve

based upon $N(E)$ and that based upon $R(\omega)$ are in reasonable agreement. It is now apparent that the peak near -5 eV in $\omega\sigma(\omega)$ is due to the peak at -4.6 eV in N_V. The principal difference between the curve obtained here and that obtained by Ehrenreich, Philipp, and Olechna[7] is the additional structure which appears in our curve but not in that of Ref. 6 for $\hbar\omega < 3.0$ eV. This difference might be due to direct transitions or to varying momentum matrix elements[26]; however, it should be noted that the $\sigma(\omega)$ data of Ehrenreich, Philipp and Olechna is based upon a Kramers-Kronig analysis of the reflectance. It is possible to lose structure in this analysis because of its complexity. It should also be noted that structure appears in the reflectivity data (Fig. 16) for $\hbar\omega < 3.0$ eV reminiscent of that obtained in our calculated curve.

A density of states for paramagnetic Ni and Ni-Cu alloys near the Fermi level has been calculated by

Fig. 16. The reflectance of nickel, after Ehrenreich, Philipp, and Olechna (Ref. 7).

---

[25] These numbers are based upon measurements of the saturation magnetic moment of Ni and upon studies of Ni-Cu alloys assuming that the 5 spin-up $3d$-like electron bands are filled.
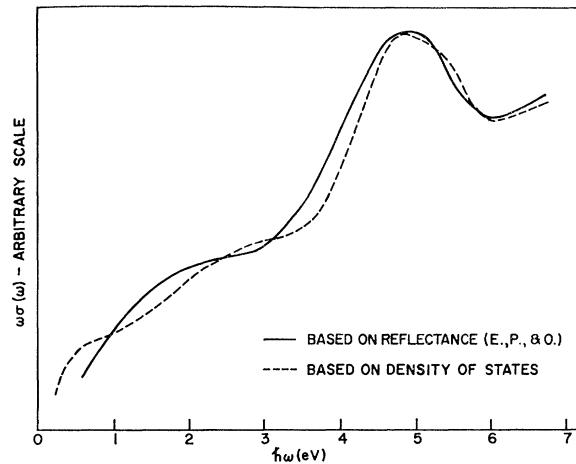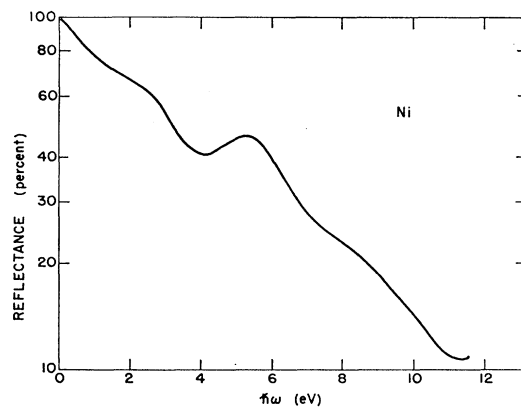
[26] It is not possible to use photoemission to check this directly since no photoelectrons are produced for $\hbar\omega < 3.0$ eV.
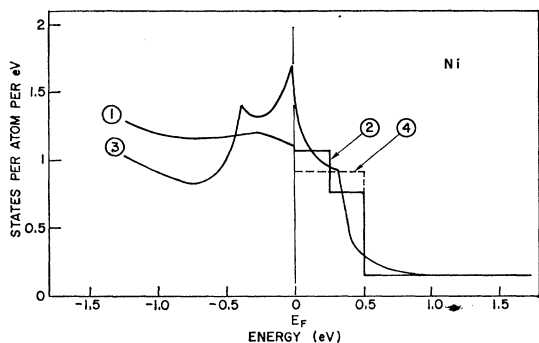
FIG. 17. The density of states in nickel near the Fermi level; curve 3 is after Shimizu, Takahashi, and Katsuki (Ref. 27). The vertical scale refers to the present work; it should be multiplied by two to give the density of states determined by Shimizu *et al.* (Ref. 27).

Shimizu, Takahashi, and Katsuki[27]; these calculations are based upon the rigid-band model and upon low-temperature specific heat measurements of Ni and Cu alloys. A density of states for ferromagnetic Ni can be obtained from the results of Ref. 27 by shifting the spin-up and spin-down bands of Ni so that their Fermi levels coincide and by summing the bands. The density of states so obtained is shown by curve 3 in Fig. 17. Curve 1 in Fig. 17 is an enlarged view of the valence-band density of states near E_F obtained from the EDC's (Fig. 11). Curve 2 is the N_C that was used to calculate $\omega\sigma(\omega)$ of Fig. 15, and curve 4 is an earlier approximation to N_C (see Appendix). (The assignment of an absolute scale to curves 1 and 2 is discussed below.)

D. The Complete Density of States

The complete density of states of Ni is plotted on an absolute scale in Fig. 18. This scale (electrons per atom per eV) was determined for N_V by assigning 10 electron states per atom to the region $-6 \leq E - E_F \leq 0$ eV. Since only the relative value of $\sigma(\omega)$ was calculated from these results, only the relative density of states above the Fermi level was involved. As a result, the magnitude of the density of states above the vacuum level has been
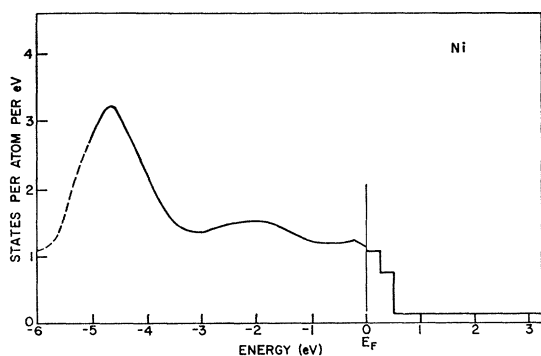

FIG. 18. The density of states in nickel.

[27] M. Shimizu, T. Takahashi, and A. Katsuki, J. Phys. Soc. Japan **18**, 801 (1963).

chosen arbitrarily. The valence-band density of states was obtained directly from the EDC's without any attempt to correct for the effects of scattering. As mentioned in Sec. VA, scattering would reduce the sharpness of peaks in the density of states and would increase the number of lower energy electrons. Thus, the actual structure in the density of states may be much stronger than that shown in Fig. 18, and the two higher energy peaks may lie at slightly higher energies. The lowest energy peak may be much sharper, and the area under it may be somewhat smaller.

VI. DISCUSSION OF THE RESULTS

A. The Rigid-Band Model

The theoretical and experimental literature concerning ferromagnetism in metals is both voluminous and complex. Rather than attempting to relate the present results to the complete literature, we will discuss the results of this work in terms of the rigid-band model[4,28] which in pure or modified form plays an important role in many of the recent considerations of ferromagnetic metals. In this model, it is assumed that, for the transition and noble metals lying in a single row on the periodic table, the band structures are quite similar and that the principal difference from metal to metal lies in the height to which the available electrons can fill the available bands, i.e., the position of the Fermi level. Opinions differ as to how variations in crystal structure will affect this model[4,27]; however, this problem will not affect the discussion of Cu and Ni since both have face-centered cubic crystal structures. Ferromagnetic metals are treated in the rigid-band model by assuming that the spin-up and spin-down bands are identical in shape; ferromagnetic behavior is accounted for by shifting one band in energy relative to the other band.

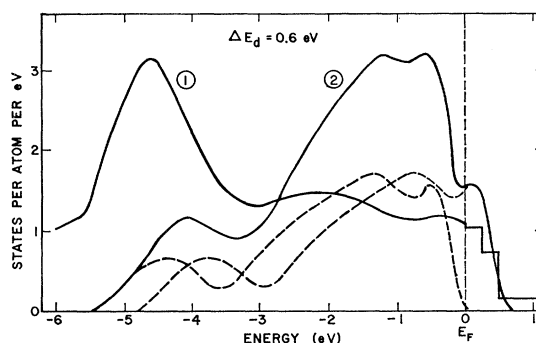Using the density of states[29] for Cu determined by

FIG. 19. The density of states in nickel; curve 1, determined from photoemission studies; curve 2, predicted by the rigid-band model from the copper density of states (Berglund and Spicer, Ref. 1) for an exchange splitting of 0.6 eV.

[28] J. L. Beeby, Phys. Rev. **135**, A130 (1964).
[29] It should be noted that this density of states is in general agreement with that calculated by Burdick (Ref. 6).
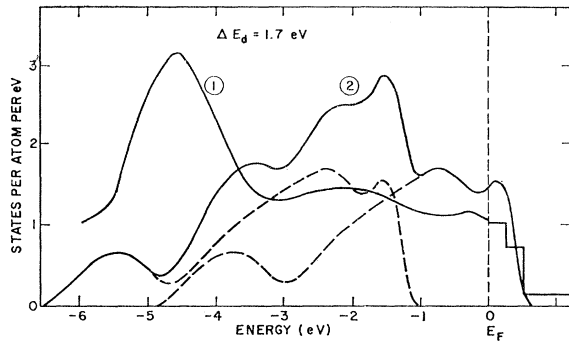
FIG. 20. The density of states in nickel; curve 1, determined from photoemission studies; curve 2, predicted by the rigid-band model from the copper density of states (Ref. 1) for an exchange splitting of 1.7 eV.

Berglund and Spicer,[1,30] and assuming the rigid-band model with an exchange splitting, ΔE, of 0.6 eV, a density of states was calculated for Ni. This is plotted in Fig. 19 (curve 2) along with the density of states for Ni determined in this work (curve 1). To obtain curve 2 from the Cu density of states, 5 spin-up and 5 spin-down electron states were assigned to two bands having the same shape as the Cu density of states (i.e., the two dashed curves in Fig. 19). The two bands so obtained were then shifted in relation to each other by an amount of energy ΔE_d and summed; the Fermi level was determined by filling 9.4 of the 10 d-like electron states (i.e., leaving 0.6 empty d-like states). The low-density s- and p-like states corresponding to the eleventh outer electron in Cu were not included in this calculation since they have a density much lower than that of the d bands.

It is apparent from Fig. 19 that the density of states predicted using the rigid-band model (curve 2) is not in agreement with that measured in this work (curve 1). The principal difference is in the strong density-of-states peak found in this work about 4.5 eV below the Fermi energy. If this was not present, reasonable agreement would have been obtained. The value of 0.6 eV for the exchange splitting ΔE_d was chosen as representative of values suggested in the literature.[31] It should be noted that the disagreement between curves 1 and 2 in Fig. 19 would become greater if ΔE_d were taken to be less than 0.6 eV. A second density of states was calculated using 1.7 eV for the exchange splitting and is shown in Fig. 20. This value for ΔE_d is perhaps the largest value suggested for the exchange splitting in Ni in the recent literature.[31] Examination of Figs. 19 and 20 should make it clear that no matter what the choice of ΔE_d may be, the density of states of Ni cannot be

obtained from that of Cu through use of the rigid-band model. In Fig. 21 the d-band density of states has been plotted for Cu and Ni with the abscissa for Cu shifted by 2 eV with respect to that for Ni. It is apparent from Fig. 21 that an important difference between the densities of states of Ni and Cu is the strong density-of-states maximum which lies approximately 4.6 eV below the Fermi level in Ni. Although there is a similar peak in Cu, it is much smaller in magnitude. No such peak was observed in Ag.[1,32,33]

Although the test of the rigid-band model described above was made using the Cu density of states determined by Berglund and Spicer, the results and conclusions would not have been changed if Burdick's calculated density of states had been used. The recent band calculations for Ni[2-4] do not appear to have any structure which could produce the −4.5 eV density-of-states peak.

B. The Occurrence of Transitions in Which Conservation of k Is Not an Important Selection Rule

As discussed in Sec. II and elsewhere,[1,9,10,13] studies of the energy distribution of photoelectrons can be used to determine whether or not direct conservation of k is an important selection rule. No evidence has been found here, as with certain other materials,[1,9,10,13] that conservation of k is an important selection rule (i.e. KNIMP transitions dominate) for those optical transitions for which the final states lie above the vacuum level (i.e.,
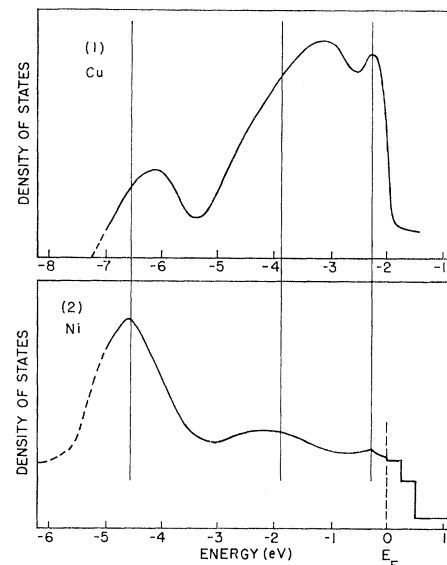

FIG. 21. Comparison of the densities of states for Cu and Ni. The zero of energy is the Fermi surface. The abscissa for Cu has been shifted by 2 eV with respect to that for Ni.

[30] A lower energy peak in the Cu energy distribution curve was observed by Berglund and Spicer but not positively identified as being due to valence-band structure (Ref. 1). More recent information suggests that it is due to a maximum in the valence-band density of states (Refs. 32 and 33). For this reason, this structure has been included in the calculation of curve 2 in Fig. 19.

[31] E. P. Wohlfarth, in *Proceedings of the International Conference on Magnetism, Nottingham, 1964* (Institute of Physics and the Physical Society, London, 1965), pp. 51–54.

[32] C. N. Berglund, Proceedings of the International Colloquium on Optical Properties and Electronic Structure of Metals and Alloys, Paris, 1965 (to be published).

[33] W. E. Spicer, Proceedings of the International Colloquium on Optical Properties and Electronic Structure of Metals and Alloys, Paris, 1965 (to be published).

for Ni, states at 4.8 eV or more above the Fermi level). Similarly, it has been shown that the principal features of the optical constant ϵ_2 can be explained in terms of KNIMP transitions.[34]

The structure in the NEDC's associated with the −4.6-eV valence-band structure could only be followed for $9.2 \lesssim \hbar\omega \leq 11.6$ eV. The lower limit was set by the minimum energy necessary to excite electrons above the vacuum level. The upper limit was set by the optical cutoff of the LiF window. Although the peak of interest in the NEDC's clearly moved to higher energies with increasing $\hbar\omega$, this movement was slower than would be expected for a nondirect transition. It has been suggested that this discrepancy is due to the effect of the escape function for final states so near the vacuum level and to the effect of scattering. This suggestion is supported by the fact that the forward edge of the peak in the NEDC's coincide quite well on the $E - \hbar\omega$ plot (Fig. 6). However, it is important to explore the possibility that this behavior is due to a direct transition. (It should be noted that even if the transition were direct it would still indicate a large number of states located approximately 4.5–5.0 eV below the Fermi level—a result of variance with band calculations and the Cu-Ni rigid-band model.) A number of things argue against a direct transition. Most important is the fact that the strongest feature in the optical constant $\omega\sigma (\epsilon_2 = \sigma/\omega)$ is well explained in terms of the density of states maximum at −4.6 eV and nondirect transitions, whereas attempts to explain it in terms of direct transitions have proved unsuccessful.[34] Thus, from the optical data evidence for the nondirect nature of the transition from the density-of-states maximum at −4.6 eV is obtained for a photon energy range ($4.5 \leq \hbar\omega \leq 7$ eV) quite different from that ($9.2 \leq \hbar\omega \leq 11.6$ eV) in which the peak is seen in the NEDC's.

A separate set of facts also argues against the strong structure in the NEDC's under discussion being due to direct transitions. A strong direct transition would require a relatively large number of final states (i.e., a high density of states) located just above the vacuum level. No independent evidence was found for such states in the energy range $6.0 \leq \hbar\omega \leq 9.2$ eV where it would have been expected (see Figs. 5–7 and 12); whereas the model proposed is consistent with all other experimental data.

As in the previous cases,[1,9,10,13] where KNIMP transitions were found to dominate, it appears that this cannot be explained simply in terms of conventional phonon-assisted transitions (i.e., indirect transitions) since, if such transitions were dominant in the energy range of

interest, the perturbation treatment on which the concept of indirect transitions is based would no longer be valid.[35] In order to avoid confusion, the term "nondirect transition" was created[1,10] to describe transitions in which conservation of **k** is not important and which cannot be explained as phonon-assisted (indirect) transitions in the conventional sense. It was pointed out in Sec. II that when the widths of the bands are comparable to the resolution characteristic of the photoemission experiment (0.1 to 0.2 eV), no distinction can be made between direct and nondirect transitions in the photoemission experiment. In the case of Ni, however, the bands extend over such a large energy range (approximately 5.0 eV) that it seems unlikely that the occurrence of KNIMP transitions can be explained simply in terms of narrow bands. It appears then that the transitions are truly nondirect.

VII. CONCLUSIONS

No evidence is found in the data obtained from the photoemission studies of Ni that conservation of wave vector **k** is an important selection rule for the range of photon energy, $6.0 \leq \hbar\omega \leq 11.6$ eV, studied (i.e. KNIMP transitions dominate). It is also found that the major features in ϵ_2 for $1 \leq \hbar\omega \leq 7.0$ eV can be explained in terms of nondirect transitions. Somewhat similar results have been reported on Cu and Ag,[1] CdS,[9] and other materials.[13] The fact that nondirect optical transitions were found to dominate in Ni for the photon energy range indicated indicates that the states involved in the optical transitions cannot be adequately described in terms of single initial and final Bloch one-electron wave functions. This may be due to localization of the hole produced in the excitation, to strong lattice interaction (less likely here than in the case of partially ionic insulators and semiconductors), or to other many-body effects.[36,37] The fact that the general shape of the $\omega\sigma$ curve (Fig. 15) is given correctly by a model based on KNIMP transitions for $\hbar\omega < 5.0$ suggests that this conclusion may hold, at least partially, for optical transitions at lower $\hbar\omega$. It should be noted, however, that the studies of Krinchik[38] of the ferromagnetic Kerr effect in Ni for $\hbar\omega \leq 1.5$ eV have been explained in terms of direct interband transitions. This suggests that the states involved in these (low photon energy) transitions are well described in terms of Bloch one-electron states and again raises the interesting possibility that direct and nondirect transitions may be dominant for transitions

[34] For a recent discussion of the optical constant, ϵ_2, of Cu in terms of direct and nondirect transitions, see: B. R. Cooper, H. Ehrenreich, and H. R. Philipp, Phys. Rev. **138**, A494 (1965); H. Ehrenreich, Proceedings of the International Colloquium on Optical Properties and Electronic Structure of Metals and Alloys, Paris, 1965 (to be published); and J. C. Phillips, in *Solid State Physics*, edited by F. Seitz and D. Turnbull (Academic Press Inc., 1966), Vol. 18, pp. 55–164.

[35] In cases where KNIMP transitions dominate (Ref. 13) and where photoemission has been obtained from cooled samples [E. A. Taft and H. R. Philipp, Phys. Rev. **115**, 1583 (1959)], the photoemission yield has been found to increase with decreasing temperature (and phonon population) in complete contradiction to what would be expected for indirect transitions.

[36] J. J. Hopfield, Phys. Rev. **139**, A419 (1965).

[37] J. C. Phillips, Phys. Rev. **140**, A1254 (1965).

[38] G. S. Krinchik, J. Appl. Phys. **35**, 1089 (1964); G. S. Krinchik and G. M. Nurmuklamedov. Zh. Eksperim. i Teor. Fiz. **48**, 34 (1965) [English transl.: Soviet Phys.—JETP **21**, 22 (1965)].

between different states in the same material, as was observed in Cu.[1,10,31,32]

It was also found that a consistent explanation of the data is possible if the momentum matrix elements for the optical transitions examined here are assumed to be constant to the first order. This result and that establishing KNIMP transitions allow determination from the photoemission data of the valence-band density of states in the energy range $-6.0 \leq (E-E_F) \leq 0$ eV (Fig. 11) and the conduction-band density of states for $5.0 \leq (E-E_F) \leq 11.6$ eV. The most striking feature of the experimentally determined density of states is the strong maximum located 4.6 eV below the Fermi level. Weaker maxima are found at about 0.3 and 2.2 eV below the Fermi surface. The conduction-band density of states was found to be constant to the first approximation for $5.0 \leq (E-E_F) \leq 11.6$ eV.

Using the photoemission results in conjunction with the optical data of Ehrenreich, Philipp, and Olechna,[7] the density of states was obtained in the energy range $0 \leq (E-E_F) \leq 5.0$ eV. A relatively high density of empty states was found within 0.5 eV of the Fermi level, and approximately constant low density of states was found above this region. The optical conductivity was calculated from the density of states, using the optical selection rules determined here, and found to be in reasonable agreement with that determined by Ehrenreich, Philipp, and Olechna[7] (Fig. 15).

It was shown that the Ni density of states determined by photoemission studies (Fig. 18) cannot be reproduced from that of Cu[1] using the rigid-band model no matter what value of exchange splitting is chosen (see Figs. 19 and 20). In particular, the strong maximum at 4.6 eV below the Fermi level in Ni cannot be predicted by this model. Phillips[37] has suggested that this strong maximum as well as the weaker structure in Cu located about 6.2 eV below the Fermi level[30] and other structure deduced from the optical data are due to resonances. Mott[39] has suggested that the density-of-states peak found in Ni at -4.6 eV may be due to the presence of the $4s^3 3d^8$ states, the presence of which has been suggested previously.[40]

ACKNOWLEDGMENTS

[39] See the comments by Professor N. F. Mott at the end of Ref. 32.
[40] N. F. Mott, Advan. Phys. **13**, 325 (1964).

APPENDIX: CALCULATION OF $\omega\sigma(\omega)$

Since the method used here to determine the density of states in the region between the Fermi level and the vacuum level (Sec. VC) has not been previously reported, it is instructive to describe the procedure used in some detail. First, several $N_C(E)$ of the general form shown in curve (a) of Fig. 14 were tried with the experimentally determined valence-band density of states in Eq. (6) and led to poor agreement with the observed $\omega\sigma(\omega)$.[7] Therefore, this form was abandoned. Next, $N_C(E)$ of the form shown in curve (b) (Fig. 14) were tried with considerable success. The parameter E_d, which corresponds to the width of the empty d-like states, was varied to obtain the proper position of the peak in $\omega\sigma(\omega)$, and the parameter δ, which corresponds to the amplitude of the d-like density of states relative to that of the lower density s- and p-like states, was varied to obtain the proper "peak-to-valley" ratio. The
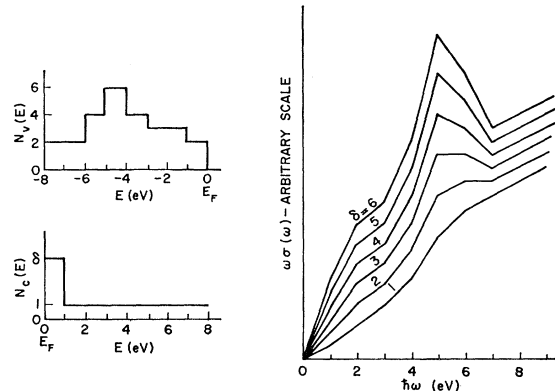

FIG. 22. Evaluation of $\omega\sigma(\omega)$.

sensitivity of this method is indicated by the calculations outlined in Fig. 22.

The curves shown on the right of Fig. 22 were calculated using Eq. (6). The histograms shown on the left were used to approximate N_V and N_C; it should be noted that the relative scales shown on these histograms are completely arbitrary, any scale factor between N_C and N_V enters $\omega\sigma(\omega)$ as a multiplicative constant—see Eq. (6). The relatively crude calculations outlined in Fig. 22 show that, for N_V of the form observed in Ni, a sizeable peak is required in N_C to explain the peak observed in $\omega\sigma(\omega)$ (Fig. 15). These curves (Fig. 22) also indicate that the calculated $\omega\sigma(\omega)$ depends strongly upon the relative amplitude parameter δ. Refined calculations indicate that, for N_C of the form indicated by curve (b) of Fig. 14, E_d should be approximately 0.5 eV and the parameter δ should be approximately 6 to obtain the best agreement with the $\omega\sigma(\omega)$ determined from reflectance.[7] Curve (c) of Fig. 14 represents a further refinement of this calculation.